Chemistry & Biology 13, 1061–1069, October 2006 DOI 10.1016/j.chembiol.2006.08.009

Evolution of High-Branching Deoxyribozymes from a Catalytic DNA with a Three-Way Junction

William Chiuman[1] and Yingfu Li[1,*]
[1] Department of Biochemistry and Biomedical Sciences and Department of Chemistry
McMaster University
1200 Main Street West
Hamilton, Ontario L8N 3Z5
Canada

Summary

Here, we report the evolution of two star-shaped (five-way junction) deoxyribozymes from a catalytic DNA containing a three-way junction scaffold. The transition was shown to be a switch rather than a gradual progression. The star-shaped motifs, surprisingly, only took five selection cycles to be detected, and another four to dominate the evolving population. Chemical probing experiments indicated that the two deoxyribozymes belong to the same family despite noticeable variations in both the primary sequence and the secondary structure. Our findings not only describe the evolution of high-branching nucleic acid structures from a low-branching catalytic module, but they also illustrate the idea of deriving a rare structural motif by sampling the sequence variants of a given functional nucleic acid.

Introduction

The advent of SELEX (an in vitro selection procedure) [1–3] has generated a plethora of aptamers [4], ribozymes [5, 6], and deoxyribozymes [7, 8]. These artificial nucleic acids have been exploited to develop molecular tools [9, 10], provide insights into nucleic acid structures [11–13], devise models for molecular evolution [14], and support the "RNA world" hypothesis [15]. Among these pursuits, our lab is interested in the development of fluorescence-signaling deoxyribozymes as potential biosensors [16].

We previously optimized six deoxyribozymes, named OA-I to OA-VI, that all contain a three-way junction framework and are able to cleave a lone RNA linkage sandwiched between a fluorescein-labeled deoxyribothymidine (dT) and a DABCYL-labeled dT [17]. Although the optimized deoxyribozymes have respectful rate constants in the range of ~0.2–1.6 min^{-1}, we attempted to further fine-tune their catalytic performance by continued evolution of the early populations of the six OA deoxyribozymes under a more stringent time pressure. After seven selection cycles, a few additional deoxyribozyme sequences have emerged along with the parent sequences in four of the six OA lineages (data not shown). Interestingly, two of these sequence classes from the OA-IV population were found to have five-stem structures arranged in a star-like configuration. In this study, we conducted in-depth analyses of these two sequence classes to establish their metal-ion requirement profiles, kinetic properties, and secondary structures. The mechanism behind the transition from the three-way junction structure of the parent deoxyribozyme to the five-way junction configuration of the star-shaped deoxyribozymes will also be discussed.

Results and Discussion

In Vitro Evolution Uncovered Five-Way Junction Motifs

The starting pool (G0) contained ~10^{14} sequence variants of OA-IV with a degeneracy of 0.3 (70% wild-type nucleotide and 10% each of the remaining nucleotides per position) [17]. Each variant was comprised of a 56 nucleotide random region flanked by 2 constant sequence elements: the 3′-primer binding site and the chimeric DNA/RNA substrate, which also included the 5′-primer binding site. The oligonucleotides were challenged to perform the cleavage of the lone RNA linkage within 60 min in the solution containing 1× selection buffer (SB) (1× SB; 50 mM HEPES [pH 6.8] at 23°C, 400 mM NaCl, 100 mM KCl, 7.5 mM $MgCl_2$, 5 mM $MnCl_2$, 1.25 mM $CdCl_2$, 1 mM $CoCl_2$, and 0.25 mM $NiCl_2$). Active molecules were isolated by denaturing polyacrylamide gel electrophoresis (PAGE), based on the faster gel mobility of shortened sequences, and were subsequently PCR amplified. Self-cleaving constructs were regenerated from the PCR products (see Experimental Procedures) and subjected to the next cycle of selection and amplification. In our previous work [17], five additional rounds of selection were performed with the reaction time decreased from 10 min in G1 to 1 min in G2–G5, and one representative clone from G6, namely, 3J-22, was thoroughly examined. The k_{obs} value of 3J-22 was determined to be 0.46 min^{-1}, and the final cleavage yield was 76%.

To explore whether incorporation of mutagenesis into the selection course could further polish OA-IV to a more efficient variant, we performed PCR by using a protocol that could introduce ~10% mutation to each nucleotide position [18, 19], after rounds 4–9 over the evolution trajectory that was branched out in G4 (Figure 1A). The reaction time allowed for the evolving populations was kept at 1 min for G4–G6, but it was dropped to 6 s for the remaining generations in order to isolate the most efficient deoxyribozymes. The cleavage yield of the end pool (G11) was 6% in 6 s. Individuals were cloned from this pool and were sequenced.

Analysis of 29 clones revealed that there are, surprisingly, 4 additional sequence classes beside the major cluster that comprises the OA-IV catalytic module (data not shown). However, none of them could be recognized even by sequence alignment with any of the other five OA deoxyribozymes we previously reported, as we suspected they might just be crosscontaminants. We focused on the two dominant "unknown" sequence classes (Figure 1B) and arbitrarily chose one sequence from each class for further investigation. Our preliminary secondary-structure models of the selected deoxyribozymes, 5J-A28 and 5J-B38, are presented in Figure 2.

*Correspondence: liying@mcmaster.ca

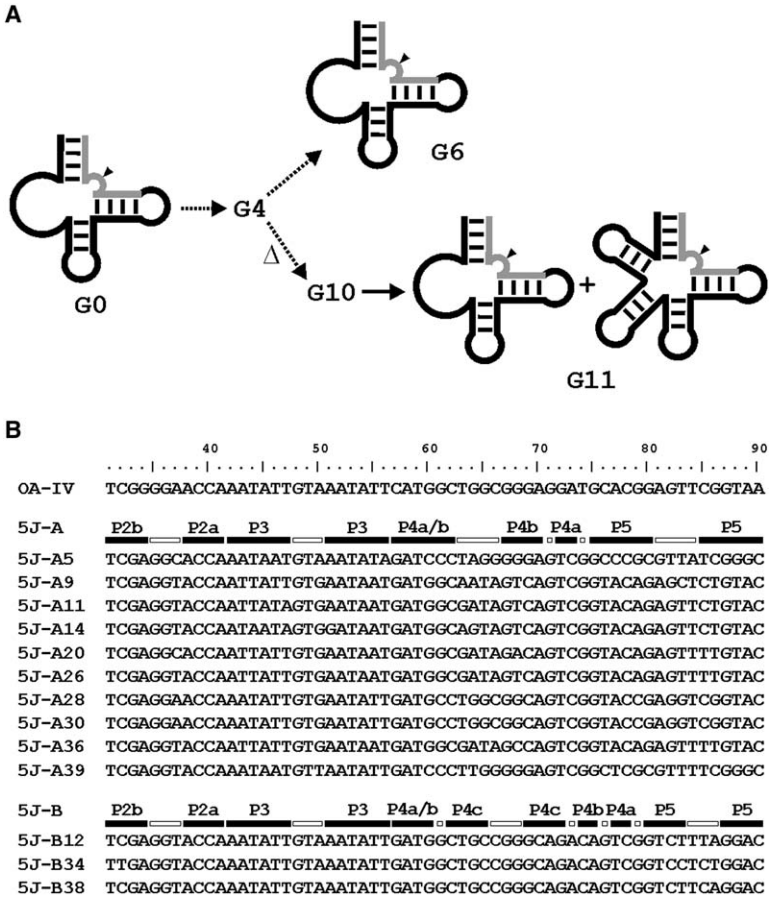

Figure 1. Identification of 5J Deoxyribozymes through In Vitro Evolution

(A) Selection trajectories of OA-IV. The selection trajectory of a partially randomized pool of OA-IV (G0) was branched into two after the third round of selection: (1) another two selection cycles were performed without any modification in the selection procedure (with regard to the previous two rounds); (2) mutations were introduced via mutagenic PCR (open triangle) after rounds 4–9, and the evolving population was challenged with increasing selection pressure by dropping the reaction time from 1 min to 6 s. Besides the deoxyribozyme having the three-way junction motif, deoxyribozymes with a bona fide five-way junction scaffold were also found in the end pool, G11. Gray and black lines represent the substrate and deoxyribozyme, respectively. The lone RNA linkage is highlighted with a black arrowhead.

(B) Sequences of the initial 13 clones of the 5J deoxyribozymes. The names fixed on the left of individual sequences designate their sequence class and clone number (e.g., 5J-A5 = 5J-class A, clone #5). The scale at the top corresponds to the nucleotide positions of deoxyribozymes located between the two PCR primer binding sites; thus, a total of 60 nucleotides were transmutable by mutagenic PCR. Filled and open bars on top of each sequence class indicate the nucleotide locations in the relevant helices and bulges/loops, respectively.

For brevity, deoxyribozymes with a five-way junction scaffold are designated as 5J-XZ, where X represents the sequence class, and Z denotes the clone number (e.g., 5J-A28 = 5J-class A, clone #28). Deoxyribozymes with an OA-IV module, thus the three-way junction scaffold, are designated as 3J-Z. Both 5J-A28 and 5J-B38 have a star-shaped, five-stem structure, wherein helix 1 (P1) is derived from the Watson-Crick pairings between the substrate and the 3′-primer binding site, which was unintentionally designed in the starting pool. The assemblage of P2 and P3 in both 5J deoxyribozymes is essentially the same as that in 3J-22. This

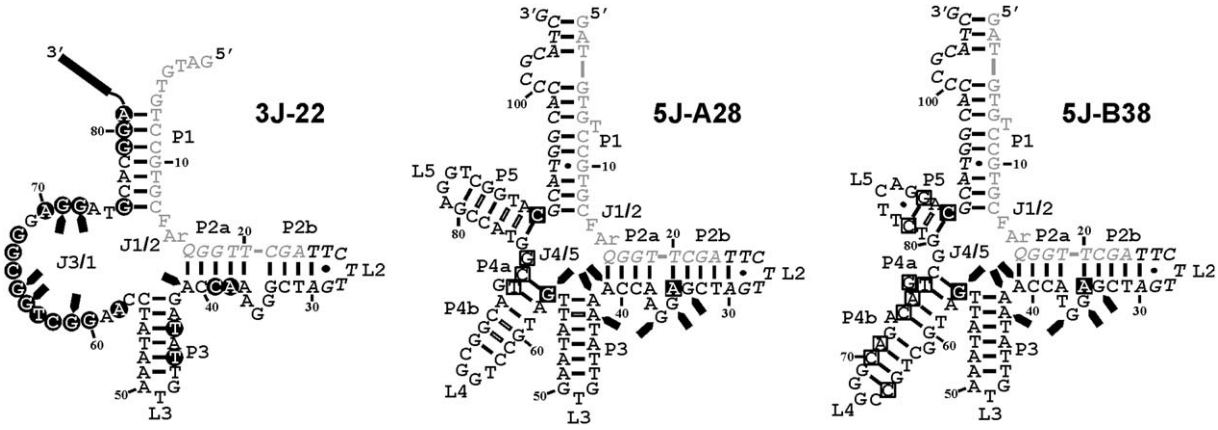

Figure 2. Structural Models of Representative 3J and 5J Deoxyribozymes

A structure model of 3J-22 [17] is shown for comparison with 5J. Highly conserved residues (>90% occurrence in all G6 clones) of 3J are highlighted with filled circles. The redundant sequence of 3J-22 is displayed as a long, solid bar at its 3′ end. Common mutations to either class or both classes of 5J deoxyribozymes, based on all of the sequenced clones of 5J (Figure S4), are highlighted with open squares and filled squares, respectively. Watson-Crick and G-T wobble base pairs are designated with short, black dashes and small, black dots, respectively. Watson-Crick interactions between covariable residues are accentuated with open bars (not shown in 3J-22). Nucleotides intolerable to methylation are indicated with solid arrows. Primer binding sites are italicized. F, fluorescein-dT; Ar, ribo-adenylate; Q, DABCYL-dT.

strongly suggests that these sequence classes were descended from the OA-IV lineage, but not from any other deoxyribozyme species in our laboratory that might somehow contaminate the OA-IV pool. The origins of P4 and P5 can be traced to J3/1 (the long junction of P3 and P1) along with the substrate-binding arm that contributes to P1 formation in the OA-IV module (Figure 2, 3J-22). Since the number of nucleotides within the interhelical junctions (J1/2 and J4/5) only adds up to three in both 5J-A28 and 5J-B38, the overall structures of the 5J deoxyribozymes are very compact.

Despite the very limited number of clones (Figure 1B), several covarying base pairs have been found in P3, P4b, and P5 of 5J-A (Figure 2), and one covarying pair was found in P5 of 5J-B. In combination with the fact that our models also coincide with the lowest-energy structures predicted by *mfold* [20], with the exception of P4a, which did not exist in the *mfold*-postulated structures, we believe that the newly emerged deoxyribozymes indeed fold into the five-stem structure to mediate their catalytic functions.

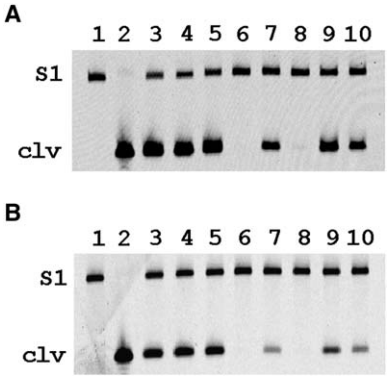

Figure 3. Metal-Ion Requirement Profiles of 5J-A and 5J-B

(A and B) Substrate S1 was cleaved by (A) 5J-A28 and (B) 5J-B38 into a 5′ cleavage fragment (denoted as "clv") that can be observed by fluorimaging. M(I) = Na + K; M(II) = Mg + Mn + Cd + Co + Ni; lane 1, no reaction; lane 2, S1 cleaved by NaOH; lane 3, M(I) + M(II); lane 4, Na + M(II); lane 5, K + M(II); lane 6, M(I) + Mg; lanes 7–10, M(I) + Mg + other individual M(II) (lanes 7–10 contain Mn, Cd, Co, and Ni, respectively). See Experimental Procedures for details.

5J-A and 5J-B Belong to the Same Deoxyribozyme Family

As implied from the sequences and structures of 5J-A28 and 5J-B38 (Figure 2), there seems to be no striking difference between sequence class A and class B, which prompted us to consider whether they actually contain the same catalytic module. It is difficult to postulate, however, at this point if the catalytic core is composed of the conserved nucleotide residues that are located at several stem vertices surrounding the center of the five-stem structure (especially the open ends of P4, which contain the same sequence context but are derived from different nucleotide positions in 5J-A and 5J-B, i.e., A_{70}–C_{73} and A_{75}–C_{78}, respectively), as there is not enough statistical data to underscore their catalytic significances.

To determine if 5J-A and 5J-B utilize the same catalytic solution to solve the same chemical problem, DMS (dimethyl sulfate) methylation interference assays [21] were performed to investigate if the N7 atoms of some guanines and the N3 atoms of some adenines were critically involved in the structural arrangements or catalytic functions of 5J-A28 and 5J-B38. There are, in theory, three different ways for these specific atoms to affect the deoxyribozyme activity when they are methylated: (1) tertiary interaction (presumably hydrogen bonds for either catalytic or structural involvement) with a distant site is hindered; (2) the optimal arrangement of nucleotides proximal to a concerned purine is impaired due to steric clashes; (3) the optimal electronic environment surrounding the concerned purine is altered with an additional positive charge. Nucleotide residues that interfered substantially with the self-cleavage activities of 5J-A28 and 5J-B38, when methylated, are highlighted with filled arrows in Figure 2 (see Figure S1 for experimental data; see the Supplemental Data available with this article online). It is clear from the distribution of filled arrows that methylation interference occurred at the same set of purines in both deoxyribozymes, suggesting that the global folds of 5J-A and 5J-B are built from a similar array of local and distal interactions. Interestingly, these purines are mainly located in P2 and P3, which were inherited from the OA-IV module as discussed earlier. Yet, the primary region of 3J-22 that was intolerable to methylation is J3/1 (Figure 2), which has become part of P4 in either 5J-A or 5J-B through evolutionary adaptation. This indicates that the catalytic contributions of P2 and P3 vary, depending on the structure landscape they are situated in. This also implies that 3J and 5J have very different structural arrangements even though they originate from the same lineage.

Metal-ion requirement profiles for the featured deoxyribozymes were also obtained by conducting 10 min cleavage assays, by using substrate S1 (5′-GATGTG TCCGTGCFArQGGTTCGATCAAGAGAATT-3′; F represents fluorescein-dT; Ar, ribo-adenylate; Q, DABCYL-dT) and the *trans*-acting 5J-A28 and 5J-B38, in a range of conditions that did not contain certain components of the selection buffer. *Cis*-to-*trans* conversions of the deoxyribozymes were made similarly by breaking loop L2 (Figure 2) and extending stem P2b with extra base pairs such that a stable P2b was created. The reaction mixtures were analyzed by denaturing PAGE, and the relevant fluorimages are shown in Figure 3. S1 alone (lane 1) has a low level of fluorescence due to fluorescence quenching by DABCYL. The 5′ cleavage fragment denoted as "clv," in contrary, is highly fluorescent (lane 2) owing to separation of the fluorophore from the quencher. Cleavage activity in the selection buffer is shown in lane 3. Lanes 4–10 indicate the requirement of Na^+, K^+, Mg^{2+}, Mn^{2+}, Cd^{2+}, Co^{2+}, and Ni^{2+} for deoxyribozyme activity. Both 5J-A28 and 5J-B38 showed no selectivity for the monovalent ions, and they were catalytically active only in the presence of Mn^{2+}, Co^{2+}, or Ni^{2+}. Since such a profile is not seen in any of the 6 OA deoxyribozymes [17], nor in at least 12 other RNA-cleaving deoxyribozymes reported in the literature [22, 23], it is unlikely that it is purely coincidental that 5J-A and 5J-B share the same metal ion requirement profile.

With similar sequence context around the center of the five-stem structure, the same cluster of nucleotides that interfere with deoxyribozyme activity when they are

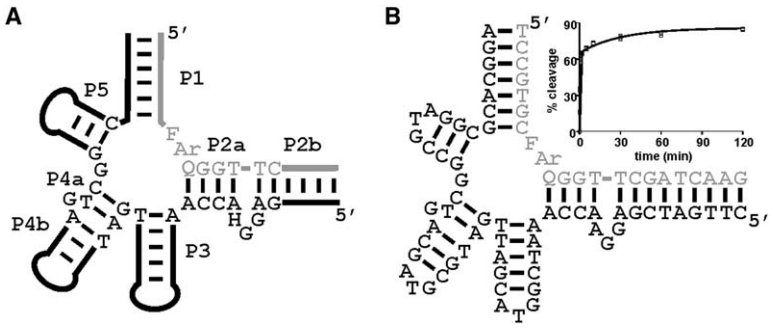

Figure 4. The Conserved Structure of 5J and the Refined 5J-A28

(A) A consensus structure model of 5J. Conserved nucleotides for both 5J-A and 5J-B are shown. Stem loops or helices of variable nucleotide contents are indicated as solid lines connected by bars that denote Watson-Crick interactions. H = A, C, or T.

(B) Improved 5J-A28 in the *trans* format. The inset shows the single-turnover kinetics of the improved 5J-A28 toward substrate S1 under an optimized condition. The experimental data were fitted into a double exponential equation, which yields $k_1 = 2.96\ min^{-1}$, $Y_{f1} = 65\%$; $k_2 = 3.27 \times 10^{-2}\ min^{-1}$, $Y_{f2} = 21\%$. See Experimental Procedures for details.

methylated, and the identical metal-ion requirement profile, it is reasonable to conclude that 5J-A and 5J-B belong to the same deoxyribozyme family.

Validating the Secondary Structures of 5J-A28

We have chosen 5J-A as our model to further verify the secondary structures of the 5J deoxyribozymes simply because more sequenced clones of 5J-A than 5J-B appeared in G11 (Figure 1B), which seems to suggest that 5J-A had more selective advantages (presumably better folding and faster kinetics) over 5J-B in the course of evolution. In addition, there are more base pair covariation data available for 5J-A (Figure 2), which could assist the design of mutant variants intended for assessing the catalytic significances of stems P3, P4, and P5. Briefly, individual stem loops were incorporated separately with deletions, substitutions, mismatches, and alternate Watson-Crick pairings in a series of deoxyribozyme constructs. Both 5 and 15 min cleavage assays were carried out in *trans* by adding deoxyribozymes to various substrates that were preincubated in the selection buffer. Cleavage yields with regard to modifications of a particular stem loop were compared. Details of individual mutant constructs and experimental results are presented in Figures S2 and S3. A summary of the results will be described below.

All helices (P1–P5) were found to be required for deoxyribozyme activity. Deletion of either DNA strand of any helix or incorporation of several mismatches within the stem motifs was detrimental to catalytic function. The sequence contexts of P1 and P2 can be changed as long as equivalent Watson-Crick base pairs are retained. However, P2 could only be altered in the window of L2 to the $G_{22} \equiv C_{32}$ pair in P2b (Figure 2, 5J-A28). Modifications beyond this window resulted in a significant drop in catalytic activity, indicating that P2a, the $G_{35}G_{36}A_{37}$ bulge, and the remaining two base pairs of P2b all play significant roles in catalytic function. This notion is further supported by the methylation interference results, which showed that G_{33}, G_{35}, G_{36}, and A_{41} in the aforementioned regions are intolerable to methylation. Similar to P2, P4 can only be mutated in the window of L4 to the $G_{60} \equiv C_{69}$ pair in P4b. The contents of L3, L4, and L5 are unimportant for catalysis, thus posing several good sites for biosensor engineering [24, 25]. A consensus 5J structure model is shown in Figure 4A. Nucleotides that are conserved in all of the sequenced clones of 5J-A and 5J-B are indicated (note: beside the 13 sequences shown in Figure 1B, 53 additional sequences of 5J were obtained from a total of 327 clones; see Figure S4). Adjustable stem loops or helices confirmed by characterizing 5J-A28 are depicted as solid lines connected by bars.

Our best 5J-A28 mutant, which was about twice as active as the wild-type construct (Figure S2, compare WT and DC-5), is shown in Figure 4B. In single-turnover conditions, the cleavage rate of this mutant toward substrate S1 is best described by biphasic kinetics with $k_1 = 2.96\ min^{-1}$ and $Y_{f1} = 65\%$ in the fast phase, and $k_2 = 3.27 \times 10^{-2}\ min^{-1}$ and $Y_{f2} = 21\%$ in the slow phase (Figure 4B, inset; k represents the observed rate constant; Y_f represents the final cleavage yield).

5J Outcompeted 3J over the Course of Evolution

Intrigued by the improved performance of 5J-A28 over 3J-22 (~6-fold better), we were interested in examining whether 5J was able to surpass 3J in the context of in vitro selection. To address this question, the end population (G11, Figure 1A) was subjected to two additional selection cycles, in which no additional mutations were incorporated into the population by mutagenic PCR and the reaction time was kept at 6 s. Individuals were cloned from various generations covering G7–G13 and were sequenced. Aligned sequences are shown in Figures S4 and S5. The partitions of various deoxyribozyme classes in successive generations are shown in Figure 5A. "NR" in the figure represents sequences that could not be recognized by using the highly conserved sequence modules and the conserved stem loop motifs of the 5J and all OA deoxyribozymes. An accelerated growth in pool fractions of 5J accompanied with a quick drop in 3J (Figure 5A) clearly indicates that 5J competed better under the stringent time pressure. Interestingly, 5J-B, which appeared in higher abundance in early generations, was later outcompeted by 5J-A in G11 and onward. This suggests that the mutational steps required for the conversion of 3J to 5J-B were less than those required for 5J-A. However, 5J-A eventually became more dominant, presumably owing to its better biochemical properties.

Although the surviving DNA molecules were selected based on their self-cleavage capability within the restricted time, it is unclear whether other factors such as PCR amplification efficiency might overpower the competency of the deoxyribozyme and sway the pool distribution contrarily to our expectation. To investigate

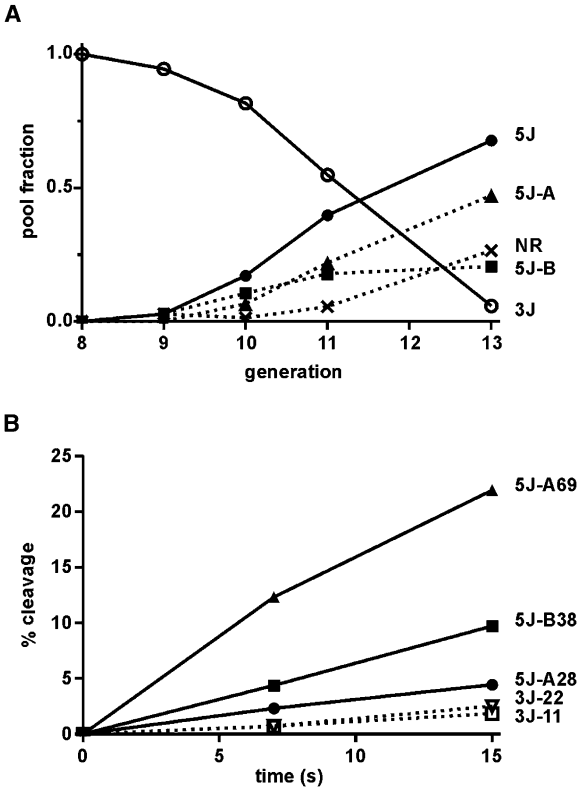

Figure 5. Cleavage Kinetics as One of the Selection Forces behind the Competition between 3J and 5J

(A) Distribution of deoxyribozymes over the course of evolution. 5J includes both 5J-A and 5J-B. NR = not recognizable sequences. Pool fractions of 3J and 5J over consecutive generations are connected by solid lines to emphasize their fall and rise, respectively. Pools prior to G8 were dominated by 3J (data not shown). The plot was derived from a total of 267 clones over G8–G13.

(B) The first 15 s of self-cleavage reactions of some representative 3J and 5J deoxyribozymes. Reactions were carried out in 1× SB with 50 nM deoxyribozyme. Cleavage assays for each time point were repeated in at least three independent experiments, and the data are presented as the means plus standard deviation. Cleavage yields of 3J and 5J deoxyribozymes over time are connected by a broken line and a solid line, respectively.

if faster cleavage kinetics, as a dominant trait by itself, is able to elucidate the selection mechanism behind the competition between 3J and 5J, *cis* cleavage assays were carried out in 1× SB, by using several clones arbitrarily selected from G6* (the asterisk refers to the normal selection trajectory, where no PCR mutagenesis was applied) and G11. In brief, the self-cleavage rates of the 3J deoxyribozymes showed a monophasic behavior with relatively slower kinetics than the 5J deoxyribozymes, which were at least 2.6× more efficient in the fast phase of the cleavage reactions, given that their self-cleavage rates all showed biphasic behavior (Figure S6). Figure 5B pinpoints the differences in cleavage yield between the 3J and 5J deoxyribozymes over the time frame relevant to the reaction time allowed in G7–G12. Despite a large variation in the cleavage rate and cleavage yield of the selected 5J-A deoxyribozymes, the fact that 5J, in general (as exemplified by 5J-A28, 5J-A69, and 5J-B38), had better kinetics and cleavage yield than 3J in the beginning of the time course strongly indicates that faster cleavage kinetics was a critical trait to develop in order to survive in a rigorous evolution landscape.

It is noteworthy that 5J, particularly 5J-B, took only five rounds of selection and amplification to be detected (Figure 5A, G9) after PCR mutagenesis was first introduced into the selection procedure. For a functional oligonucleotide to be discovered from a complete random library, the number of selection cycles required typically falls in the range of 4–20 cycles [7, 8]. With only a 6-fold difference between 3J-22 and 5J-B38 (or even a 12-fold difference between 3J-22 and 5J-A69) in terms of the cleavage yield in the first 7 s of the reactions (Figure 5B), faster cleavage kinetics could certainly not account for the entire selection force that directed the population distribution to favor 5J in such a rapid pace. This prompted us to wonder if 5J could have existed in the starting population and accumulated to a detectable amount over many generations. The probability (P) for 5J-B to appear in G0 (a synthetic library with a degeneracy of 0.3) was estimated to be 6.4×10^{-19} ($P = [0.7]^{40} \times [0.1]^{12}$), based on the 40 highly conserved residues (>90% occurrence) and 12 common mutations with regard to the starting sequence (Figure S4). For a population of $\sim 10^{14}$ molecules (G0), it is very unlikely that 5J-B could have existed in the synthetic library. Although there might have been 6527 molecules of 5J-A (based on the 27 highly conserved residues and 6 common mutations) in the starting pool, the fact that 5J-A actually appeared later than 5J-B in the evolution trajectory is an indication that 5J-A also did not exist in G0. At this point, we do not have any experimental evidence to imply that there are other selection forces that might act on the competition between 3J and 5J. Further deconvolution of the acting forces is a challenge to overcome before the mechanism behind in vitro evolution can be better understood.

Transition of 3J to 5J

With sequence information compiled from 327 clones of 3J, 5J-A, and 5J-B dispersed over G6* and G7–G13, here we attempt to evaluate the evolutionary distance from 3J to 5J (distance here refers to the number of mutations required for a 3J deoxyribozyme to convert into either 5J-A or 5J-B). For convenience, we use "EM" and "BP" to designate the highly conserved nucleotides in a given 5J class, which do not overlap with those in 3J, and mutations that are required for the formation of new Watson-Crick base pairs (including G-T wobbles), respectively. In the 3J → 5J-A trajectory, we have identified seven EMs (A_{34}, G_{57}, T_{59}, T_{72}, C_{73}, G_{74}, and C_{90}) and seven BPs (G_{60}-C_{69}, C_{61}-G_{68}, T_{76}-A_{89}, A_{77}-T_{88}, C_{78}-G_{87}, C_{79}-G_{86}, and G_{80}-C_{85}). In the 3J → 5J-B pathway, we have found eight EMs (A_{34}, G_{57}, T_{59}, A_{75}, G_{76}, T_{77}, C_{78}, and C_{90}) and seven BPs (G_{69}-C_{74}, T_{63}-A_{71}, G_{64}-C_{70}, C_{65}-G_{69}, T_{81}-A_{89}, C_{82}-G_{88}, and T_{83}-G_{87}). Therefore, the total number of mutations required for 3J/5J-A and 3J/5J-B conversions is 14 and 15, respectively (note: a base pair is counted as one mutation instead of two).

We next normalize the required EMs and BPs such that 5J-A and 5J-B will have a value of 1 in both EM and BP. The averages of the normalized EMs and BPs attained by individual clones from G6* and G7–G9 are shown in Figure 6A (3J → 5J-A pathway) and Figure 6B

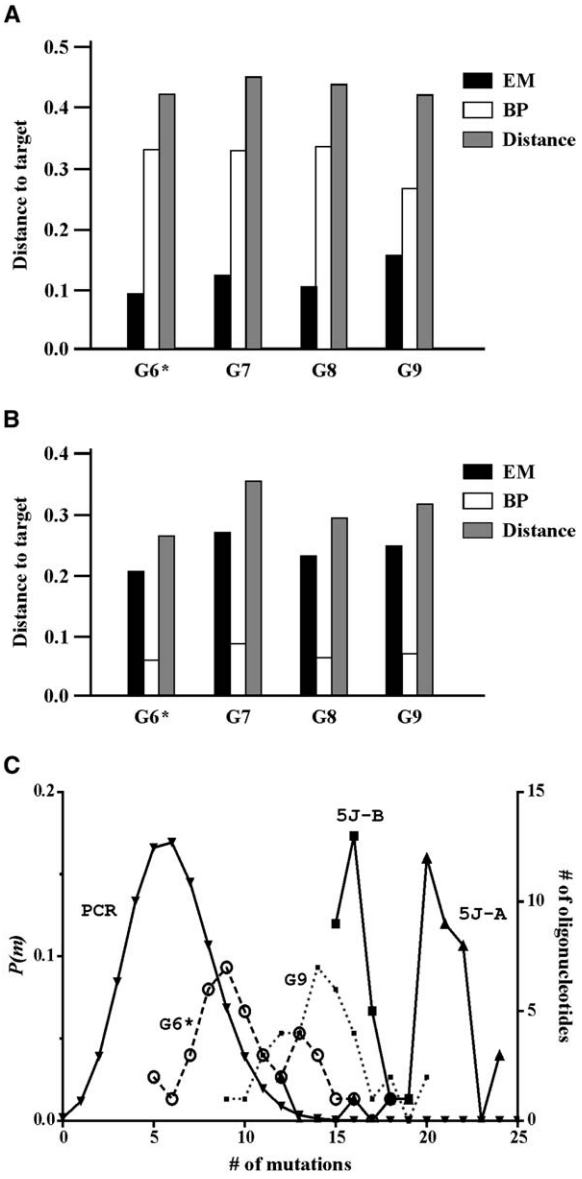

Figure 6. Analysis of the Evolutionary Distance from 3J to 5J as well as Mutation Frequencies over the Course of Evolution

(A and B) Averaged distances from 3J to (A) 5J-A and (B) 5J-B. There are two types of mutations: the ones that are essential for the catalytic function of 5J (EM), and the ones that create Watson-Crick base pairs necessary for the secondary structures of 5J (BP). The total EMs and BPs that a 3J deoxyribozyme would acquire to convert into 5J-A (equally 7) and 5J-B (8 and 7, respectively) are normalized to 1. The average value of normalized EM, BP, and EM + BP (distance) attained by the sequenced clones in G6* and G7–G9 are shown as black, white, and gray bars, respectively.

(C) Mutation frequencies over the course of evolution and in the populations that consist of 5J deoxyribozymes. Probability distribution of oligonucleotides with "m" number of mutations (P(m), solid, upside-down triangle), as a result of one PCR mutagenesis procedure, refers to the left y axis. See Experimental Procedures for P(m) derivation. Mutation frequencies with respect to the starting sequence (OA-IV) in G6* (open circle), G9 (small, filled squares), and all of the sequenced clones of 5J-A (solid triangle) and 5J-B (large, filled squares) refer to the right y axis. Mutation frequencies in G7 and G8, and the mutation frequencies falling outside the range of occurrences, are not shown for clarity. The averaged mutations in G6* and G7–G9 are 10.2, 12.4, 13.0, and 14.2, respectively. 5J-A and 5J-B have an average of 20.4 and 16.0 mutations, respectively. Note that G6* and G7–G9 are populated mostly by 3J deoxyribozymes, with the exception of one single 5J-B found in G9. This 5J-B sequence is not taken into account in order to minimize statistical errors.

(3J → 5J-B; see the figure legend for details), which reveal several interesting trends: (1) the overall distance for a 3J/5J-A or 3J/5J-B transition does not change significantly over the evolution trajectory; (2) the EM value for 5J-A is smaller than that for 5J-B in every generation; (3) in contrast, the BP value for 5J-A is larger than that for 5J-B.

The first trend described above suggests that each 3J/5J transition is not a gradual process, but perhaps a sudden switch event. The switch model is also consistent with an observation at the sequence level, where specific positions along the DNA sequence have a different conserved nucleobase identity for 3J and 5J-A (or 5J-B). For example, at position 72, there is a need for guanine in 3J, but thymine in 5J-A. Similarly, at position 75, 3J must have a guanine, but 5J-B requires an adenine (Figure 2). These conserved nucleotide incompatibilities create apparent conflicts that make it difficult for 3J to make a gradual transition to 5J. The incompatibilities may, in turn, force the transition to proceed by the switch mechanism.

We interpret the markedly different EMs (and BPs) for the 3J/5J-A and 3J/5J-B transitions as the differential potential of the evolving population to take on either of the two transitions. The observation that 5J-B emerged earlier than 5J-A (Figure 5A) suggests that it might be easier for the evolving population to employ the evolutionary pathway favored by more EM mutations. This supports the idea that the likelihood for a particular motif to be found from a region of distinct compositional space is influenced, in the order of higher significance, by the probability to find the global folding, flanking helices, and conserved bases [26].

To analyze the mutational behavior of the evolving deoxyribozyme variants, we have calculated the mutation frequencies that occurred in all of the sequenced 3J and 5J clones with respect to the starting sequence OA-IV (which was used as the basis for the creation of a degenerate library by chemical synthesis). The data, along with the probability of sequences having different numbers of mutations generated by the mutagenic PCR, are shown in Figure 6C.

Two points can be made from the analysis of the data in Figure 6C. First, the PCR mutagenesis indeed introduced more mutations into 3J variants along the selection course. This is evident from comparison of the frequency curve of the 3J variants in G6* (open circle) with that in G9 (small solid square). For clarity, the data for G7 and G8 variants are omitted. Second, we believe that the strategy of evolving a degenerate deoxyribozyme library produced by chemical mutagenesis, followed by further incorporation of mutations with mutagenic PCR, will facilitate the isolation of rare deoxyribozyme motifs such as 5J-A and 5J-B. We have already discussed in the previous section that it is unlikely that we can isolate the 5J deoxyribozymes from the synthetic library. Our calculation indicates that the mutagenic PCR protocol is able to generate all possible

sequence variants with up to only 10 mutations plus increasingly smaller fractions of the sequence variants with higher errors (note: this calculation was made on the assumption that the PCR procedure in each selection round could generate $\sim 10^{13}$ molecules). Considering DNA polymerase's strong bias for making transition over transversion errors in the mutagenic condition [18, 19], the actual coverage of all possible sequence variants could be even smaller. Since the number of mutations in 5J-A (solid triangle) and 5J-B (large solid square) clones mainly fall in the range of 20–22 and 15–17, respectively, it is hard to imagine that mutagenic PCR alone could easily generate such hypermutated variants.

Implications for Evolutionary Biology and Biotechnology

The abundance and diversity of functional nucleic acids (abbreviated as FNA) in a given sequence space have important implications on the output of an in vitro selection experiment and the "RNA world" hypothesis. The abundance has been demonstrated by a plethora of nucleic acid aptamers and enzymes that were identified in nature and created artificially in laboratories. The diversity on the structural level, however, has hardly been explored. It has been suggested by a computational study that a random sequence library, regardless of its size, heavily favors simple topological structures such as linear stem loops and low-branching motifs [27]. The current compilation of FNAs clearly illustrates that perception [4, 6, 7, 23, 28]. As a consequence, the variety of chemical problems that can be solved by nucleic acids will always be constrained by the same cluster of simple structural modules. Here, we trained the deoxyribozyme OA-IV that contains the most common three-way junction scaffold found in a wide variety of FNAs [17, 23, 28–30] to perform better in catalyzing an RNA-cleavage reaction by changing its genotype with mutagenic PCR. The result was a more complex secondary structure with five stems in a star-like configuration accompanied by improved cleavage kinetics. Such a peculiar configuration was also found in the peptidyl transferase center of 23S ribosomal RNA [31] and the recently identified lysine riboswitch [32, 33], but it was never found in any FNA isolated by in vitro selection. Hence, there is definitely a range of complex functional motifs that are yet to be discovered but with an unconventional strategy.

Previous strategies to create artificial FNAs typically involved a complete random library of different lengths [8] or a hypervariable sequence with a built-in structural domain [34–37]. In some cases, the optimization of the isolated FNAs was performed by incorporating light mutation (1%–10% per position) via mutagenic PCR. Since the development of new functions and altered ligand specificities [38, 39] was usually the objective of previous studies, the sequence diversity within a particular FNA class was not explored to evolve a new functional motif. Although our initial objective was to further optimize deoxyribozyme OA-IV, the idea of evolving a rare multibranching motif from a relatively simple secondary structure is illustrated here. The evolution of alternative catalytic modules that were identified in several OA lineages (data not shown), including OA-IV, strongly encourages the search for new functions by sampling the sequence space (or the so-called "neutral network" [40, 41]) of a given FNA. The rationale behind this is that if a few sequence variants of a particular FNA initially contain base compositions that are biased toward forming alternative structures, these sequences could be transformed into a new functional motif by structural rearrangement with the aid of appropriate mutations supplied by mutagenic PCR. Alternatively, a degenerate library of an existing functional module could also be used as the starting point from which to build new FNAs, as shown by previous selection efforts [42–44]. However, in our particular case, the rare 5J motifs can be reached only through some mutational pathways from a few specific coordinates in the sequence space of the 3J motif.

Recent advances in biosensing technology and nanotechnology have exploited nucleic acid aptamers and enzymes as the sensing and signaling platforms for the detection of a specific target [24, 45]. The helical and stem-loop motifs of a nucleic acid enzyme are usually the sites for sensor coupling. However, since the contents of these regions in most enzymes cannot be altered, as a significant drop in catalytic activity would be compromised, the number of targets that could be detected concurrently would be very limited. Here, we present a deoxyribozyme that can potentially be equipped with up to five sensors and give a fluorescence-signal output upon target binding. We believe the high-branching configuration of 5J will be put to good use in sensing and signaling applications.

Significance

The present study describes how a deoxyribozyme supported by the three-way junction (3J) framework was converted into the five-way junction (5J) structures, which have better catalytic performance, through evolutionary pathways. The in vitro evolution of such high-branching motifs has expanded the structural diversity of nucleic acids with a catalytic function. The 3J-to-5J transition involved the preservation of two helical stems and structural rearrangement of the original catalytic core, which later acquired several mutations in order to compete better under a more stringent selection pressure. The catalytic contribution of the two preserved stems, however, differs in the 3J and 5J scaffolds of the deoxyribozymes. These again indicate the high plasticity of nucleic acids to adopt different structural folds from a pre-existing structure if provided with appropriate mutations. Analyzing the origins of 5J deoxyribozymes suggests that a highly intricate structure may only be isolated through the evolution of some sequence variants of an ancestor with a simpler secondary structure, rather than directly from a completely random library or from a degenerate library. Perhaps, this less-explored strategy to search for new structural motifs will find great use in future selection experiments.

Experimental Procedures

In Vitro Evolution

A portion (~20%) of the G4 population (see Figure 1A for the selection trajectory) was PCR amplified in a volume of 50 μl containing 75 mM Tris-HCl (pH 9.0), 2 mM $MgCl_2$, 50 mM KCl, 20 mM $(NH_4)_2SO_4$,

0.2 mM each of the four dNTPs, 1.25 U *Thermus thermophilus* DNA polymerase, 0.5 μM DNA primer 1 (5′-TTACATCTACAA ACATGGTTCGATTCTTGA-3′) and 0.5 μM DNA primer 2 (5′- CGATG CGGGTGCCATGC-3′). The PCR was carried out for 10 thermocycles during which the temperature was altered in the following order: 94°C, 30 s (2 min for the first cycle); 45°C, 45 s; 72°C, 45 s. A small portion (~10^{-3}%) of the PCR products was amplified in the second PCR by using a similar condition to that described above, but with 0.3 μM primers 2 and 3 (5′-TTACATCTACAAACATGGTTCGAr-3′), for 15 cycles of 94°C, 30 s (2 min for the first cycle); 53°C, 45 s; 72°C, 45 s. Radiolabeling of the pool was conducted in a manner similar to that of the second PCR, but with 3 μM each of the four dNTPs, 10 μCi [α-^{32}P]dGTP, 0.2 μM primers 2 and 3, in a total volume of 25 μl. To introduce ~10% mutations per nucleotide position, mutagenic PCR was performed in parallel for 20 cycles of 94°C, 30 s (2 min for the first cycle); 53°C, 45 s; 72°C, 90 s. The mutagenic condition was adapted from the protocol reported by Vartanian et al. [18] and is described as follows: 20 mM Tris-HCl (pH 8.4), 50 mM KCl, 2.5 mM $MgCl_2$, 0.5 mM $MnCl_2$, 30 μM dATP and dCTP, 1 mM dGTP and dTTP, 0.05 U/μl *Thermus aquaticus* DNA polymerase, 0.3 μM primers 2 and 3, and a small portion (≤10^{-3}%) of the first PCR products. Mutagenic PCR amplification was performed after rounds 4–9 in the evolution trajectory. The proportion of mutated sequences, wherein the mutations were incorporated by mutagenic PCR, and nonmutated sequences was varied from round to round in various arbitrary ratios; rounds 4–9, 3:1, 3:2, 3:2, 2.4:1, 1:1.2. Mutagenic and nonmutagenic PCR products were combined and ethanol precipitated. The pellet was resuspended in 90 μl of 0.25 M NaOH and was incubated at 90°C for 10 min to cleave the single ribonucleotide linkage (Ar) within one of the two strands. A total of 10 μl of 3 M NaOAc (pH 5.2) was subsequently added to neutralize the solution. The cleaved DNA strand was isolated by 10% denaturing PAGE, eluted from the gel, and ethanol precipitated. To restore the DNA into the self-cleaving construct, the DNA was first 5′ phosphorylated by using T4 polynucleotide kinase (PNK). It was then annealed to the chimeric DNA/RNA substrate (5′-GATGTGTCCGTGCFArQGGTT CGA-3′) by using a DNA splint and T4 DNA ligase. The ligated oligonucleotides were purified by 10% denaturing PAGE and resuspended in H_2O.

The oligonucleotide solution was heated at 90°C for 30 s and cooled at room temperature for ~10 min. The self-cleavage reaction was carried out with ~0.1 μM oligonucleotide in 1× selection buffer (SB) (1× SB; 50 mM HEPES [pH 6.8] at 23°C, 400 mM NaCl, 100 mM KCl, 7.5 mM $MgCl_2$, 5 mM $MnCl_2$, 1.25 mM $CdCl_2$, 1 mM $CoCl_2$, 0.25 mM $NiCl_2$). The reaction was stopped after 1 min by adding EDTA (pH 8.0 at 23°C) to a final concentration of 30 mM. The self-cleaved oligonucleotides were separated from the inactive species by 10% denaturing PAGE and were used as the templates for PCR amplification, so as to begin the next selection cycle. Eight additional rounds of selection were performed as described above, except that the reaction time was shortened to 6 s. G7–G11 and G13 populations were cloned and sequenced for further analyses.

Metal Ion Requirements

Metal ion requirements for deoxyribozyme activity were determined by comparing the cleavage activities in *trans* in a range of reaction conditions that did not carry certain components of the selection buffer. Cleavage reactions were initiated by adding deoxyribozyme (optimized 5J-A28 [Figure 4B] or nonoptimized 5J-B38) to S1 (see Supplemental Experimental Procedures for its making), which was preincubated in one specific buffer. The final concentration of each constituent in the reaction mixtures was as follow: 5 nM S1, 250 nM deoxyribozyme, 50 mM HEPES buffer (pH 6.8 at 23°C), different proportions of monovalent and divalent metal ions with reference to Figure 3: lane 3, M(I) + M(II) (M(I) represents 400 mM NaCl and 100 mM KCl); lane 4, 400 mM NaCl + M(II) (M(II) represents all divalent metal ions in the same concentrations as in 1× SB); lane 5, 100 mM KCl + M(II); lane 6, M(I) + 15 mM $MgCl_2$; lane 7, M(I) + 5 mM $MnCl_2$ + 10 mM $MgCl_2$; lane 8, M(I) + 1.25 mM $CdCl_2$ + 13.75 mM $MgCl_2$; lane 9, M(I) + 1 mM $CoCl_2$ + 14 mM $MgCl_2$; lane 10, M(I) + 0.25 mM $NiCl_2$ + 14.75 mM $MgCl_2$. The reactions were stopped after 10 min or 2 hr (data not shown, as similar profiles were observed) by adding EDTA (pH 8.0) to 30 mM. Lane 1 is a control of no cleavage. Lane 2 shows the full cleavage of S1 by NaOH; that is, 5 nM S1 was incubated in 0.25 M NaOH for 10 min at 90°C, followed by neutralization with 0.3 M NaOAc (pH 5.2). The oligonucleotides in all reaction mixtures were precipitated with ethanol before analyses by 10% denaturing PAGE. For fluorimaging, the excitation wavelength on the variable mode imager was set to 532 nm (green laser), while the emission was monitored at >535 nm by using a long-pass filter. Cleavage fractions were quantitated only from phosphorimages by using the Molecular Dynamics software (data not shown).

Kinetic Analyses

Self-cleavage assays were carried out with 50 nM deoxyribozyme in 1× SB at room temperature. Deoxyribozyme was first heat denatured in H_2O at 90°C for 30 s, and it was then cooled at room temperature for ~10 min. Reactions were initiated by mixing a deoxyribozyme with the selection buffer, and they were stopped after a designated period of time by adding EDTA (pH 8.0) to 30 mM. For *trans* reactions, 750 nM deoxyribozyme was combined with 5 nM substrate S1 in an optimized reaction condition (50 mM HEPES [pH 7.0], 1 mM $CoCl_2$, 10 mM $MnCl_2$, 1 × 10^{-3} % Tween 20). Higher deoxyribozyme concentrations did not considerably enhance the catalytic rate, indicating that 750 nM deoxyribozyme was saturating (data not shown). The reactions were stopped in a manner similar to that described above. Cleavage products from both *cis* and *trans* reactions were separated by 10% denaturing PAGE and quantitated by using a phosphorimager and the Molecular Dynamics software. The *cis* kinetic experiments were conducted over 10 time points over the course of 2 hr, while the *trans* cleavage assays were conducted over 12 time points over the course of 5 hr. Cleavage assays for each time point were repeated in at least three independent experiments. The cleavage fraction was plotted versus time and fitted to either a single ($Y = Y_f [1 - e^{-kt}]$) or a double ($Y = Y_{f1}[1 - e^{-k1t}] + Y_{f2}[1 - e^{-k2t}]$) exponential equation with $R^2 > 0.99$ by using GraphPad software Prism 4.03. Y represents cleavage yield; Y_f represents final cleavage yield; k represents the observed rate constant.

Calculating P(m)

$P(m) = u^{r-m} \bullet (1 - u)^m \bullet {}_rC_m$, where P is the probability of having oligonucleotides with m mutations as a result of one PCR mutagenesis procedure; u = 0.9 (fraction of unchanged nucleotides per position); r = 60 (randomizable region; see Figure 1B); ${}_rC_m$ = a combinatorial function of r taking m at a time, i.e., the total number of possible combinations for m in the randomizable region.

Supplemental Data

Supplemental data include methods for oligonucleotide preparation, DMS methylation interference assays, and secondary structure characterization, as well as figures for DMS methylation interference patterns of selected 5J-A and 5J-B, secondary structure characterization of 5J-A28, alignment of cloned sequences over the course of evolution, and *cis* kinetic data relevant to 3J-11, 3J-22, 5J-A28, 5J-A69, and 5J-B38. These data are available at http://www.chembiol.com/cgi/content/full/13/10/1061/DC1/.

Acknowledgments

This work was supported by a research grant from the Canadian Institutes for Health Research. Y.L. is a Canada research chair. W.C. is a Clifton W. Sherman Graduate Scholarship holder. The authors declare that there are no competing financial interests.

Received: July 13, 2006
Revised: August 11, 2006
Accepted: August 25, 2006
Published: October 20, 2006

References

1. Ellington, A.D., and Szostak, J.W. (1990). In vitro selection of RNA molecules that bind specific ligands. Nature *346*, 818–822.
2. Robertson, D.L., and Joyce, G.F. (1990). Selection in vitro of an RNA enzyme that specifically cleaves single-stranded DNA. Nature *344*, 467–468.

3. Tuerk, C., and Gold, L. (1990). Systematic evolution of ligands by exponential enrichment: RNA ligands to bacteriophage T4 DNA polymerase. Science *249*, 505–510.
4. Lee, J.F., Hesselberth, J.R., Meyers, L.A., and Ellington, A.D. (2004). Aptamer database. Nucleic Acids Res. *32*, D95–D100.
5. Wilson, D.S., and Szostak, J.W. (1999). In vitro selection of functional nucleic acids. Annu. Rev. Biochem. *73*, 791–836.
6. Fiammengo, R., and Jaschke, A. (2005). Nucleic acid enzymes. Curr. Opin. Biotechnol. *16*, 614–621.
7. Achenbach, J.C., Chiuman, W., Cruz, R.P., and Li, Y. (2004). DNAzymes: from creation in vitro to application in vivo. Curr. Pharm. Biotechnol. *5*, 321–336.
8. Joyce, G.F. (2004). Directed evolution of nucleic acid enzymes. Annu. Rev. Biochem. *73*, 791–836.
9. Sun, L.Q., Cairns, M.J., Saravolac, E.G., Baker, A., and Gerlach, W.L. (2000). Catalytic nucleic acids: from lab to applications. Pharmacol. Rev. *52*, 325–347.
10. Breaker, R.R. (2004). Natural and engineered nucleic acids as tools to explore biology. Nature *432*, 838–845.
11. Lin, C.H., and Patel, D.J. (1997). Structural basis of DNA folding and recognition in an AMP-DNA aptamer complex: distinct architectures but common recognition motifs for DNA and RNA aptamers complexed to AMP. Chem. Biol. *4*, 817–832.
12. Patel, D.J., Suri, A.K., Jiang, F., Jiang, L., Fan, P., Kumar, R.H., and Nonin, S. (1997). Structure, recognition and adaptive binding in RNA aptamer complexes. J. Mol. Biol. *272*, 645–664.
13. Patel, D.J., and Suri, A.K. (2000). Structure, recognition and discrimination in RNA aptamer complexes with cofactors, amino acids, drugs and aminoglycoside antibiotics. J. Biotechnol. *74*, 39–60.
14. Schultes, E.A., and Bartel, D.P. (2000). One sequence, two ribozymes: implications for the emergence of new ribozyme folds. Science *289*, 448–452.
15. Muller, U.F. (2006). Re-creating an RNA world. Cell. Mol. Life Sci. *63*, 1278–1293.
16. Mei, S.H., Liu, Z., Brennan, J.D., and Li, Y. (2003). An efficient RNA-cleaving DNA enzyme that synchronizes catalysis with fluorescence signaling. J. Am. Chem. Soc. *125*, 412–420.
17. Chiuman, W., and Li, Y. (2006). Revitalization of six abandoned catalytic DNA species reveals a common three-way junction framework and diverse catalytic cores. J. Mol. Biol. *357*, 748–754.
18. Vartanian, J.P., Henry, M., and Wain-Hobson, S. (1996). Hypermutagenic PCR involving all four transitions and a sizeable proportion of transversions. Nucleic Acids Res. *24*, 2627–2631.
19. Weill, L., Louis, D., and Sargueil, B. (2004). Selection and evolution of NTP-specific aptamers. Nucleic Acids Res. *32*, 5045–5058.
20. Zuker, M. (2003). Mfold web server for nucleic acid folding and hybridization prediction. Nucleic Acids Res. *31*, 3406–3415.
21. Shen, Y., Brennan, J.D., and Li, Y. (2005). Characterizing the secondary structure and identifying functionally essential nucleotides of pH6DZ1, a fluorescence-signaling and RNA-cleaving deoxyribozyme. Biochemistry *44*, 12066–12076.
22. Liu, Z., Mei, S.H., Brennan, J.D., and Li, Y. (2003). Assemblage of signaling DNA enzymes with intriguing metal-ion specificities and pH dependences. J. Am. Chem. Soc. *125*, 7539–7545.
23. Silverman, S.K. (2005). In vitro selection, characterization, and application of deoxyribozymes that cleave RNA. Nucleic Acids Res. *33*, 6151–6163.
24. Breaker, R.R. (2002). Engineered allosteric ribozymes as biosensor components. Curr. Opin. Biotechnol. *13*, 31–39.
25. Silverman, S.K. (2003). Rube Goldberg goes (ribo)nuclear? Molecular switches and sensors made from RNA. RNA *9*, 377–383.
26. Knight, R., De Sterck, H., Markel, R., Smit, S., Oshmyansky, A., and Yarus, M. (2005). Abundance of correctly folded RNA motifs in sequence space, calculated on computational grids. Nucleic Acids Res. *33*, 5924–5935.
27. Gevertz, J., Gan, H.H., and Schlick, T. (2005). In vitro RNA random pools are not structurally diverse: a computational analysis. RNA *11*, 853–863.
28. Tang, J., and Breaker, R.R. (2000). Structural diversity of self-cleaving ribozymes. Proc. Natl. Acad. Sci. USA *97*, 5784–5789.
29. Santoro, S.W., and Joyce, G.F. (1997). A general purpose RNA-cleaving DNA enzyme. Proc. Natl. Acad. Sci. USA *94*, 4262–4266.
30. Lescoute, A., and Westhof, E. (2006). Topology of three-way junctions in folded RNAs. RNA *12*, 83–93.
31. Polacek, N., and Mankin, A.S. (2005). The ribosomal peptidyl transferase center: structure, function, evolution, inhibition. Crit. Rev. Biochem. Mol. Biol. *40*, 285–311.
32. Rodionov, D.A., Vitreschak, A.G., Mironov, A.A., and Gelfand, M.S. (2003). Regulation of lysine biosynthesis and transport genes in bacteria: yet another RNA riboswitch? Nucleic Acids Res. *31*, 6748–6757.
33. Sudarsan, N., Wickiser, J.K., Nakamura, S., Ebert, M.S., and Breaker, R.R. (2003). An mRNA structure in bacteria that controls gene expression by binding lysine. Genes Dev. *17*, 2688–2697.
34. Jaeger, L., Wright, M.C., and Joyce, G.F. (1999). A complex ligase ribozyme evolved in vitro from a group I ribozyme domain. Proc. Natl. Acad. Sci. USA *96*, 14712–14717.
35. Davis, J.H., and Szostak, J.W. (2002). Isolation of high-affinity GTP aptamers from partially structured RNA libraries. Proc. Natl. Acad. Sci. USA *99*, 11616–11621.
36. Ohuchi, S.J., Ikawa, Y., Shiraishi, H., and Inoue, T. (2002). Modular engineering of a Group I intron ribozyme. Nucleic Acids Res. *30*, 3473–3480.
37. Yoshioka, W., Ikawa, Y., Jaeger, L., Shiraishi, H., and Inoue, T. (2004). Generation of a catalytic module on a self-folding RNA. RNA *10*, 1900–1906.
38. Lehman, N., and Joyce, G.F. (1993). Evolution in vitro of an RNA enzyme with altered metal dependence. Nature *361*, 182–185.
39. Frank, D.N., and Pace, N.R. (1997). In vitro selection for altered divalent metal specificity in the RNase P RNA. Proc. Natl. Acad. Sci. USA *94*, 14355–14360.
40. Huynen, M.A., Stadler, P.F., and Fontana, W. (1996). Smoothness within ruggedness: the role of neutrality in adaptation. Proc. Natl. Acad. Sci. USA *93*, 397–401.
41. Reidys, C., Stadler, P.F., and Schuster, P. (1997). Generic properties of combinatory maps: neutral networks of RNA secondary structures. Bull. Math. Biol. *59*, 339–397.
42. Mannironi, C., Scerch, C., Fruscoloni, P., and Tocchini-Valentini, G.P. (2000). Molecular recognition of amino acids by RNA aptamers: the evolution into an L-tyrosine binder of a dopamine-binding RNA motif. RNA *6*, 520–527.
43. Huang, Z., and Szostak, J.W. (2003). Evolution of aptamers with a new specificity and new secondary structures from an ATP aptamer. RNA *9*, 1456–1463.
44. Curtis, E.A., and Bartel, D.P. (2005). New catalytic structures from an existing ribozyme. Nat. Struct. Mol. Biol. *12*, 994–1000.
45. Navani, N.K., and Li, Y. (2006). Nucleic acid aptamers and enzymes as sensors. Curr. Opin. Chem. Biol. *10*, 272–281.